Journal of the European Ceramic Society 44 (2024) 4741–4750

Contents lists available at ScienceDirect

Journal of the European Ceramic Society

journal homepage: www.elsevier.com/locate/jeurceramsoc

Ultrafast high-temperature sintering (UHS) vs. conventional sintering of 3YSZ: Microstructure and properties

Mattia Biesuz [a,*], Thomas Hérisson de Beauvoir [b,*], Emanuele De Bona [a], Michele Cassetta [a], Charles Manière [c], Vincenzo M. Sglavo [a], Claude Estournès [b]

[a] University of Trento, Department of Industrial Engineering, Via Sommarive 9, 38123 Trento, TN, Italy
[b] CIRIMAT, Université Toulouse 3 – Paul Sabatier, CNRS-INP-UPS, Université de Toulouse, 118 route de Narbonne, 31062 Toulouse, France
[c] Normandie Univ, ENSICAEN, UNICAEN, CNRS, CRISMAT, 14000 Caen, France

ARTICLE INFO

Keywords:
Ultrafast high-temperature sintering
YSZ
UHS
Rapid sintering
Hardness
Grain boundaries

ABSTRACT

Doped-zirconia finds several applications as strucutral material and in different electrochemical devices; moreover, it is considered a model ceramic system. The consolidation of 3 mol% Y_2O_3 stabilized ZrO_2 (3YSZ) by rapid sintering (flash processes) has yielded unusual properties like higher hardness and thinner electrochemical grain boundaries. To explore the effect of high heating rate and distinguish it from field-induced phenomena, we investigated and compared UHS (Ultrafast high-temperature sintering) with conventional heating with and without an electric field.

The results show that: i) UHS allows ultra-rapid consolidation (<30 s) of YSZ nanopowders (≈20 nm) with a densification pathway different from conventional sintering in terms of microstructural evolution (UHS allows a grain size reduction by more than 60% at a fixed desnity level); ii) the electric field plays a minor role in sintering, microstructure evolution, and properties; iii) UHS does not affect the hardness and the grain boundary electrochemical properties of the sintered bodies. Whereas similarities can be pointed out between UHS and flash-related techniques in terms of accelerated densification and microstructure, the final properties are rather different with UHS YSZ being more similar to conventional sintering.

1. Introduction

In the last decades, scientific research in the field of sintering has focused on developing novel firing techniques characterized by reduced carbon footprint and energy consumption and allowing novel microstructures [1]. In this context, a particular relevance has been gained by field-assisted processes [2] like spark plasma sintering (SPS) [3–5], microwave sintering [6], flash sintering (FS) [7–10], and flash spark plasma sintering (FSPS) [11,12].

Although there is still a debate on the interaction between electromagnetic fields, point defects, and mass transport during sintering, all such technologies share a common feature: they allow rapid heating of the green component with rates that are not possible in conventional conditions. Fast heating has been shown to have beneficial effects [13,14] on densification for a set of reasons that are quite established, including (i) the possibility of cross "quickly" the low-temperature region where coarsening, and not densification, is activated [15], (ii) the development of different pore coordination (in the case of FS [16]), (iii) the reduction of the pore-grain boundary separation [17].

Nevertheless, additional effects of rapid heating are still debated. One of the most attractive is connected with the development of a substantial difference in the obtained grain boundaries structures. These "not relaxed" boundaries are thought to be characterized by different (and possibly enhanced) self-diffusion coefficients compared with the "equilibrium" counterparts obtained *via* conventional heating, thus providing a fast pathway for sintering [14]. In this regard, there is microstructural evidence (TEM) of out-of-equilibrium boundaries in alumina consolidated by self-propagating high-temperature synthesis [18] and YSZ sintered by FSPS [19] and pressure-less SPS [20]. An indirect observation of the grain boundary structure can be attained by the measurement of specific macroscopic properties. In particular, some of the authors of the present work observed that YSZ sintered by FSPS is characterized by superior hardness when compared to the conventionally sintered counterpart and thinner grain boundary (determined by electrochemical impedance spectroscopy, EIS) [19]. Similar electrochemical results were also obtained by M'Peko et al. [21] on flash

* Corresponding authors.
E-mail addresses: mattia.biesuz@unitn.it (M. Biesuz), thomas.herisson-de-beauvoir@univ-tlse3.fr (T.H. Beauvoir).

https://doi.org/10.1016/j.jeurceramsoc.2024.01.064
Received 21 September 2023; Received in revised form 17 January 2024; Accepted 19 January 2024
Available online 22 January 2024

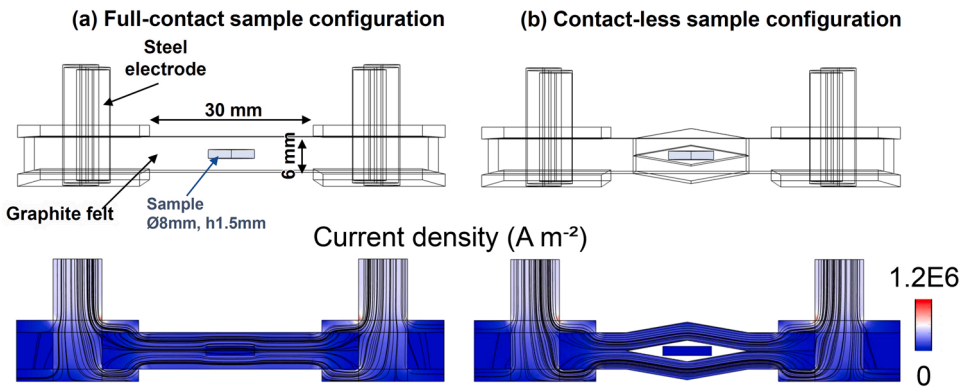

Fig. 1. Scheme of the two geometrical configurations considered in the FEM simulation of UHS: (a) "full-contact" situation with no apertures in the felt around the specimen; (b) "contact-less" situation with no contact between sample and felt and cooling convection fluxes in the internal surfaces. The current line distribution is shown below.

sintered YSZ. FSPS and FS are, however, rather "complex" process that involves not only rapid heating but also electric fields, currents, and electric power dissipation within the specimen. It is therefore still not clear how much rapid heating can account for the modified grain boundary properties [19].

In the context of rapid heating approaches, ultrafast high-temperature sintering (UHS) [22] is gaining nowadays a growing scientific and technological interest with applications embracing different families of inorganic materials [23–34]. Here, a porous heating element (usually graphite felt, although other approaches are also possible [35]) containing the ceramic sample is rapidly heated by the Joule effect to temperatures even exceeding 2000 °C.

The aim of the present work is to study UHS of a model ceramic system, 3YSZ, (i) to understand whether the UHS conditions can improve the densification of the ceramic and modify its microstructural evolution and (ii) to verify if modified electrochemical/mechanical properties are obtained (similarly to what observed in FSPS) to point out the effect of rapid heating on grain boundary conductivity and hardness.

2. Experimental procedures

US Nano company (USA) 3 mol% yttria-stabilized zirconia (3YSZ, https://www.us-nano.com/inc/sdetail/9447) powder with a particle size of 21 ± 6 nm was used. About 210 mg of powder was weighed using an analytical balance added to 20 mg of de-ionized water, the mixture being homogenized in an agate mortar with an agate pestle.

The green bodies were shaped by uniaxial pressing under 250 MPa in a steel die (diameter 8 mm, thickness ≈1.5 mm).

The UHS experiments were carried out using a graphite felt (SGL Carbon Co., Germany) which was connected to a DC power source (Agilent 6674 A). The electrode span was 30 mm and the felt cross-section was about 6 × 24 mm^2 (nominal thickness = 5 mm, measured thickness = 6mm). A small hole was created at the felt center with a spatula where the sample was introduced. The hole was then closed with a small fragment of graphite felt to reduce the heat loss. UHS was carried out using different currents in the range 18 – 26 A. Most of the experiments lasted for 30 s, although some samples were also produced by applying the current for 15 and 20 s. All UHS processes were carried out in a borosilicate glass flask where Ar vigorously flowed.

Conventional sintering experiments were carried out using a Nabertherm tubular furnace operating in with a heating and cooling rate of 20 °C min^{-1} and holding time at the maximum temperature of 30 min. In order to check the possible effect of static electric fields on YSZ sintering, the samples were processed with and without the application of 500 V cm^{-1} field, which was applied in open circuit mode (therefore, without any current passing through the sample). To apply the field, the samples were placed between two platinum electrodes connected to a DC power source (Agilent 6674 A).

The density of the sintered pellets was assessed by Archimedes' method using water as a buoyancy medium. The relative density was calculated using 6.05 g cm^{-3} as theoretical density. The microstructure was analyzed on fresh fracture surfaces by FE-SEM (Zeiss Supra40), the samples being sputtered with a thin Pt-Pd layer in advance. The grain size and pore coordination were determined on polished and thermally etched samples (UHS under 20 A and conventional heating at 1350 °C, with and without field). Sintered YSZ was polished using SiC papers up to 4000 grit and using 1 μm diamond paste. Thermal etching was carried out at 900 °C and 1250 °C for UHS and conventionally sintered materials, respectively. The pore coordination was calculated on the polished and etched surface by counting how many grains surround a given pore in the plane. At least 40 pores were considered for each sample.

The samples were observed with a scanning transmission electron microscope (S-TEM), ThermoFisher TALOS F200S (Thermo Fisher Scientific Inc., Waltham, MA, USA), at a maximum electron at the maximum electron voltage of 200 kV. TEM samples were mechanically polished on both sides down to a thickness of about 100 μm. Three-millimeter discs were obtained with an ultrasonic cutter. The final thinning down to the electron transparency was carried out in a Leica ion-millier RES102 with Ar ion, applied voltage of 7 kV, current of 2.6 mA, and incidence angle 5°.

The mineralogical analysis was carried out by X-ray diffraction on the starting powder and the sintered pellets using an Italstructures IPD 3000 diffractometer equipped with Cu anode (Kα radiation). Raman spectra were acquired at room temperature using a micro-Raman spectrometer (Horiba Jobin-Yvon LabRam HR 800) employing a He-Ne laser (632.8 nm) operating at 6 mW power with a spot size of 1.5 μm. A narrow-band notch filter was used to cut the signal from the Rayleigh line to 200 cm^{-1}. The scattered radiation was filtered by using a grating with 600 lines mm^{-1} and detected by a nitrogen-cooled CCD detector (1024 ×256 pixels) with a resolution of 0.6 cm^{-1}.

The Vickers hardness of the different pellets was determined on polished surfaces using FUTURE-TECH FM-310 microhardness tester at 1 kgf load (load dwell time = 10 s). The hardness was averaged over 10 measurements on each sample, the data are reported with error bars representing the standard deviation.

One of the main issues in UHS experiments is the determination of the real specimen temperature and the homogeneity of the heating since the specimen is located inside the graphite felt. Finite elements method (FEM) was used in the present work to simulate the UHS process. The analysis is also required because the UHS process is very quick and the sample is not necessarily at the equilibrium temperature and far from the felt temperature. The simulation procedure and the material properties are the same as those described in previous work [36]. The electrical conductivity of the felt was calibrated by simulating of the felt

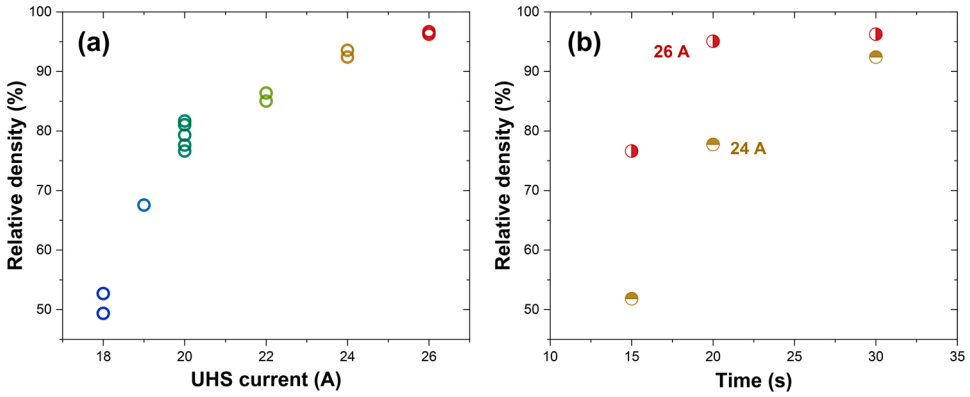

Fig. 2. Relative bulk density of UHS samples as a function of (a) applied current for 30 s treatments and (b) sintering time under 24 A and 26 A.

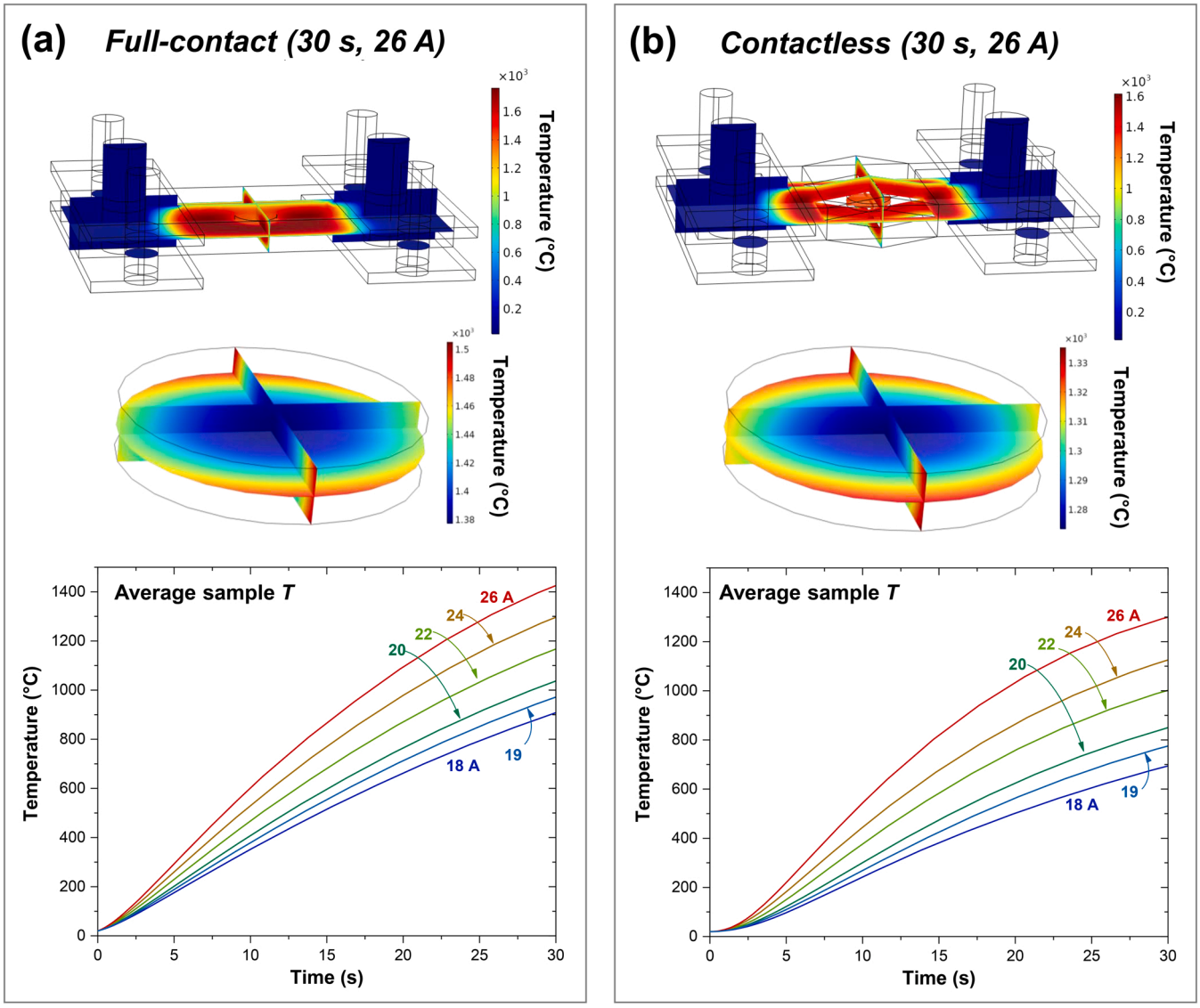

Fig. 3. FEM simulation of the UHS temperature evolution in (a) full-contact and (b) contactless model. The top line reports the temperature distribution in the felt (26 A, 30 s), the middle-line the temperature distribution in the sample (26 A, 30 s), the bottom one reports the time evolution of the average sample temperature for different currents.

heating for a wide range of imposed currents. The conductivity is then determined in the range 1000–1800 °C by checking the melting point of high-purity metals (Cu, Ni, Pt) and by matching the experimental voltage responses. The other electric and thermal properties of the felt and of the steel electrodes were taken from the literature, all the simulation parameters can be found in Table 1 in [36]. In a recent work, we

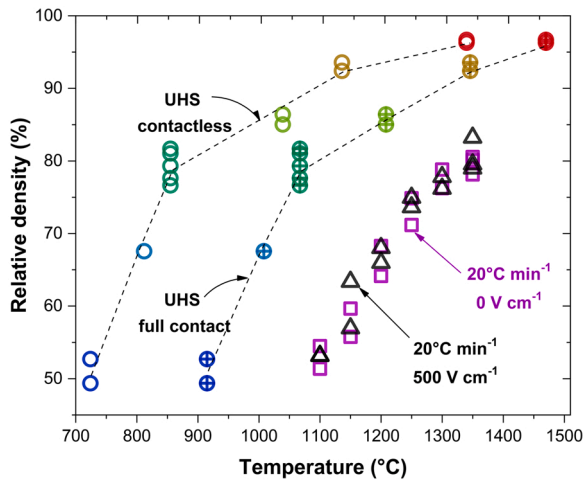

Fig. 4. Density evolution for conventionally sintered 3YSZ (with and w/o the application of static E-field) as a function of the furnace temperature; the density of UHS specimens (30 s treatments) as a function of the maximum FEM-simulated average sample temperature (data from Fig. 2) is also shown.

found a quite good agreement between the simulated temperatures and the melting point also of B_4C [37]. The UHS process is highly sensitive to convection cooling fluxes that can be fully eliminated if the felt around the sample is fully closed or high if there are apertures and leakages (chimney effect). To analyze such two extreme scenarios, the two configurations reported in Fig. 1 were considered. The former is called "full contact" and assumes a perfect contact and closure of the specimen within the felt. The other configuration is called "contact-less" and simulates the case where the sample has very poor contact with the felt and convective cooling fluxes result from apertures in the felt. For the latter, surface-to-surface thermal radiation is considered between the inner surfaces. In the present work, we considered the real specimen temperature between these two extreme cases.

Electrochemical Impedance Spectroscopy measurements were carried out in air using a Frequency Response Analyzer MTZ35 from Biologic company. Electric contacts were produced by sputtering Pt layers on specimens' surfaces. The measurements were performed in the frequency range 10^6-10^2 Hz under 100 mV peak AC current, at temperatures ranging from 400 to 200 °C. ZView software (Scribner Associates) was used for data fitting using two R-CPE in series (Resistor & Constant Phase Element).

3. Results

The relative density evolution of YSZ, determined by Archimedes'

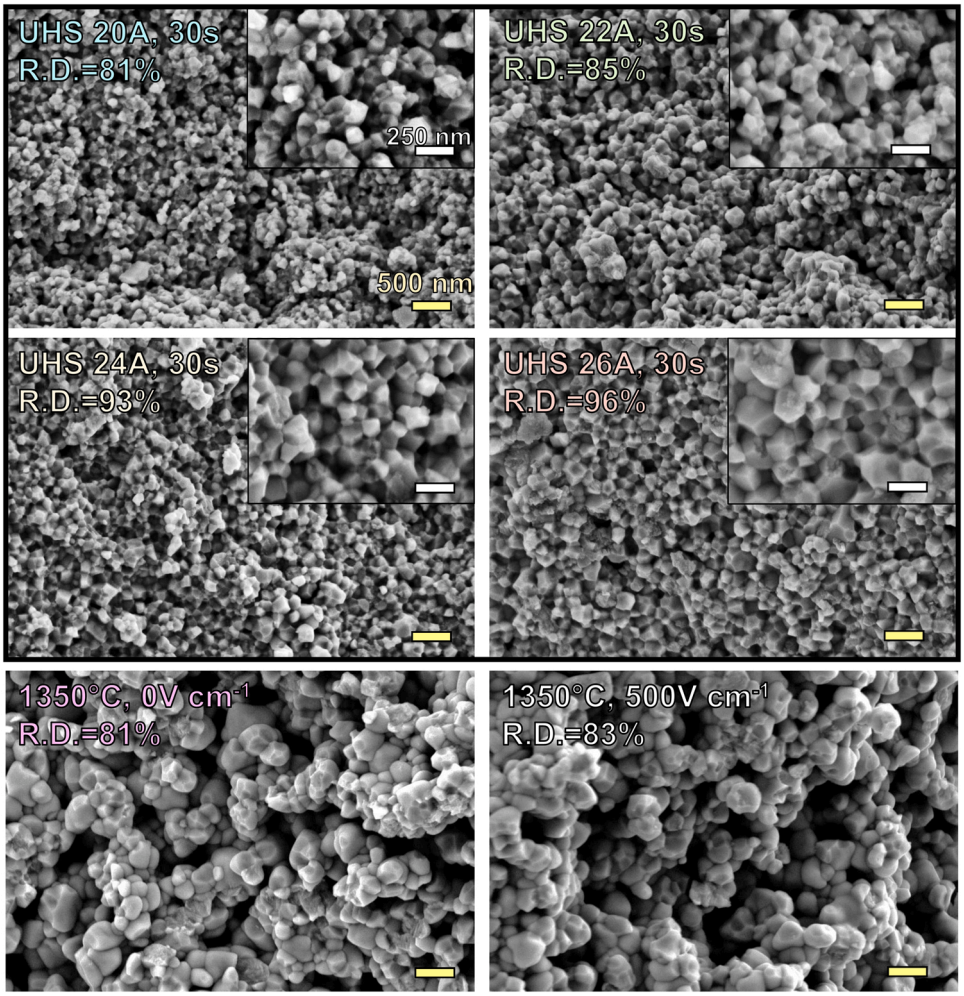

Fig. 5. SEM micrographs of UHS samples under different currents for 30 s treatment (top panel); micrographs of specimens conventionally heated without (bottom left) and with the application of a static electric field (bottom right). All micrographs refer to fracture surfaces and were taken at the sample center. The relative bulk density is also reported.

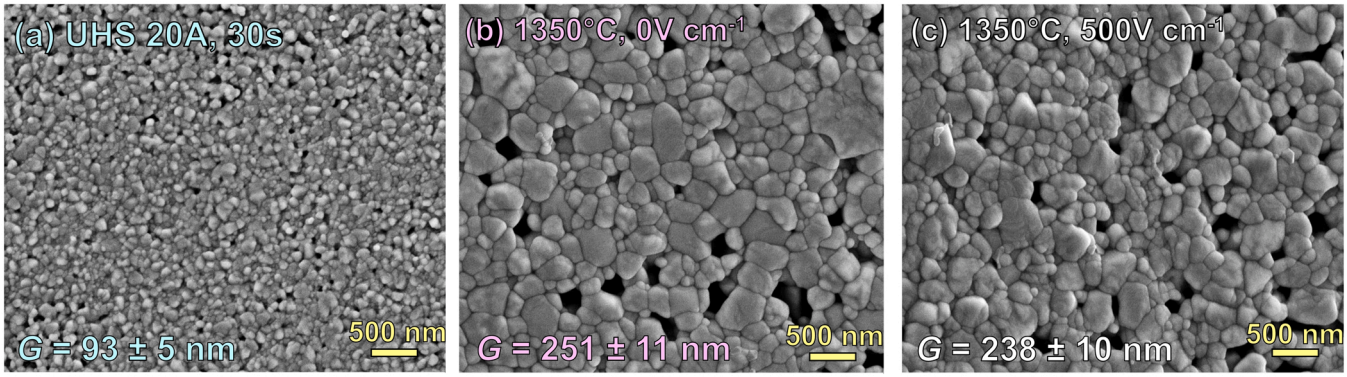

Fig. 6. SEM micrographs of polished/etched surfaces of the core of the sample processed by (a) UHS (20 A, 30 s), conventional sintering (b) without and (c) with a static electric field (500 V cm^{-1}). All samples have a relative density in the range 81–83 %; *G* represents the grain size.

method, is shown in Fig. 2 as a function of UHS conditions. We can observe that the density of the materials increases with the current from ≈ 50 % at 18A (no substantial densification compared with the green body) to ≈ 96–97 % under 26 A for 30 s. The density also grows with time, remaining modest in the first 15 s and then progressively increasing. In general, the reproducibility of the sintering process appears acceptable though UHS is clearly a "far-from-equilibrium process" (each dot in Fig. 2 represents a different specimen).

After UHS, the samples remain white for applied currents up to 20 A while their surface turns grey starting from 22 A. This color change could be associated with a partial reduction of YSZ or some carbon contamination. Based on such results, we decided to select the 20 A sample for the comparison between UHS and conventionally sintered YSZ both in terms of microstructure and electrochemical properties (so as to exclude any effect of contamination or chemical reduction).

The temperature evolution during UHS in the two considered limit configurations is reported in Fig. 3. We can observe some temperature gradients in the sample although quite modest, usually lower than 60 °C and 100 °C in the contact-less and full-contact configurations, respectively.

FEM confirms that the heating profile is extremely rapid in both the modeled conditions, allowing temperatures well above 1000 °C in less than 30 s, the final temperature increasing with processing time and current. Indeed, the heating rate is time dependent; nonetheless, we can point out that the estimated average heating rates are about 1400–1800 °C min^{-1} under 18 A (the lowest current) and could increase up to 2600–2900 °C min^{-1} under 26 A. Such heating procedures are about 2–3 orders of magnitude faster than conventional heating in a furnace.

The density of the samples sintered under conventional heating (20 °C min^{-1}) increases with the maximum temperature regardless of the application of the electric field (Fig. 4). The density evolution of UHS samples as a function of the maximum average temperature (data from Fig. 3) achieved during the treatment for both FEM models is also included in Fig. 4. We can observe that, even considering a perfect thermal contact between the felt and the sample (no temperature discontinuity at the interface between the felt and the sample), UHS induces efficient densification. Based on our previous work[37], the full contact condition might be a closer representation of the real sample temperature, however, also in this case the UHS samples densify well before the conventionally sintered ones.

SEM micrographs confirm the evident densification of UHS samples (Fig. 5) with progressive closure of the porosity at increasing applied current (20-to-26 A, 30 s treatments). In all cases, polygonal-faced grains can be observed with modest grain growth: even at the highest current (26 A) the grain size remains in the order of about 200 nm with relative density exceeding 95 %. No pores-grain boundary separation can be highlighted and the fracture mechanism remains primarily inter-

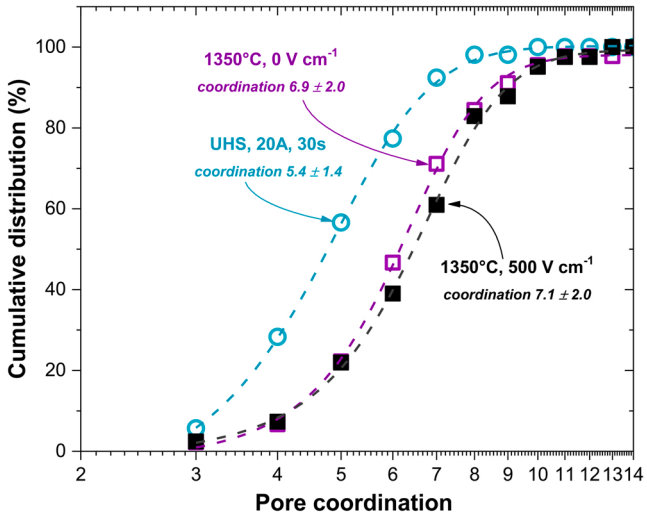

Fig. 7. Cumulative distribution of the pore coordination after conventional sintering and UHS (density ≈ 81–83 %). The average (± standard deviation) pore coordination is also shown.

granular. On the other hand, the microstructure of samples obtained by conventional heating at 1350 °C is characterized by clear coarsening phenomena, weakly dependent on the presence of a static electric field. In detail, the sample sintered at 1350 °C and the one processed by UHS under 20 A (both with a density ≈ 81–83 %) possess fairly different microstructures, the latter characterized by finer grain size. Moreover, the connectivity of the porosity and the pores coordination appear different, with larger pores coordinated by more numerous grains being evident in the conventionally sintered material.

The microstructural analysis of the polished/thermally etched surfaces (Fig. 6) confirms the differences between conventionally heated (1350 °C) and UHS (20 A) ceramics. The latter contains grains still well below 100 nm, whereas the grain size is in the order of ≈ 250 nm after conventional heating regardless of the application of an electrical field (a very modest grain refinement can be observed in the presence of the field). The pores are located at the grain boundaries in all the samples.

The pore coordination was determined from the polished/etched micrographs and it is reported in Fig. 7 through a cumulative distribution. The results point out that the pores after UHS at the same density level (≈81–83 %) are coordinated by a smaller number of grains when compared with those in the conventionally sintered zirconia. On the other hand, the differences between samples sintered without and with E-field are not significant from a statistical point of view.

The homogeneity of the UHS sample treated under 20 A was assessed

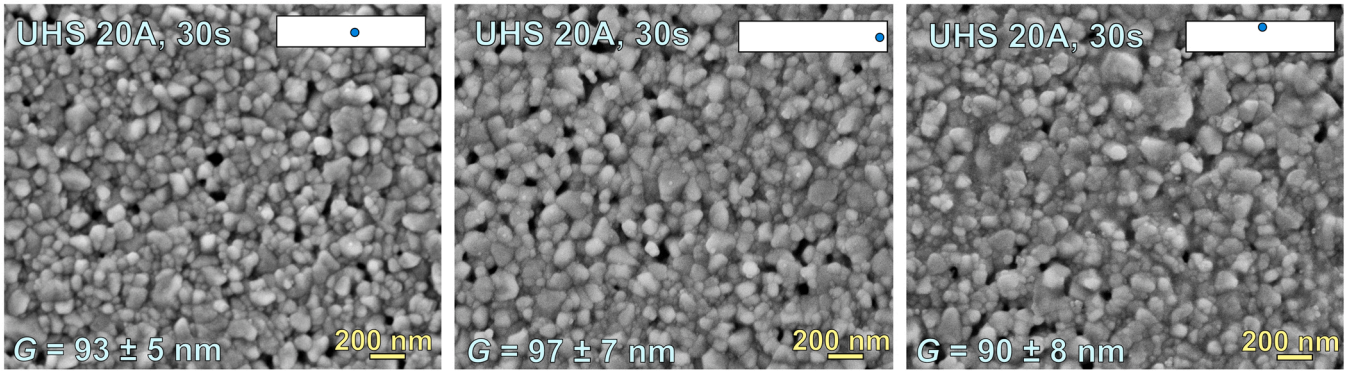

Fig. 8. SEM micrographs of polished/etched surface of different regions in the cross section of the UHS sample (20 A, 30 s). The analyzed region in the cross-section is highlighted by the blue dot in the sketch at the top right of each micrograph. *G* represents the grain size.

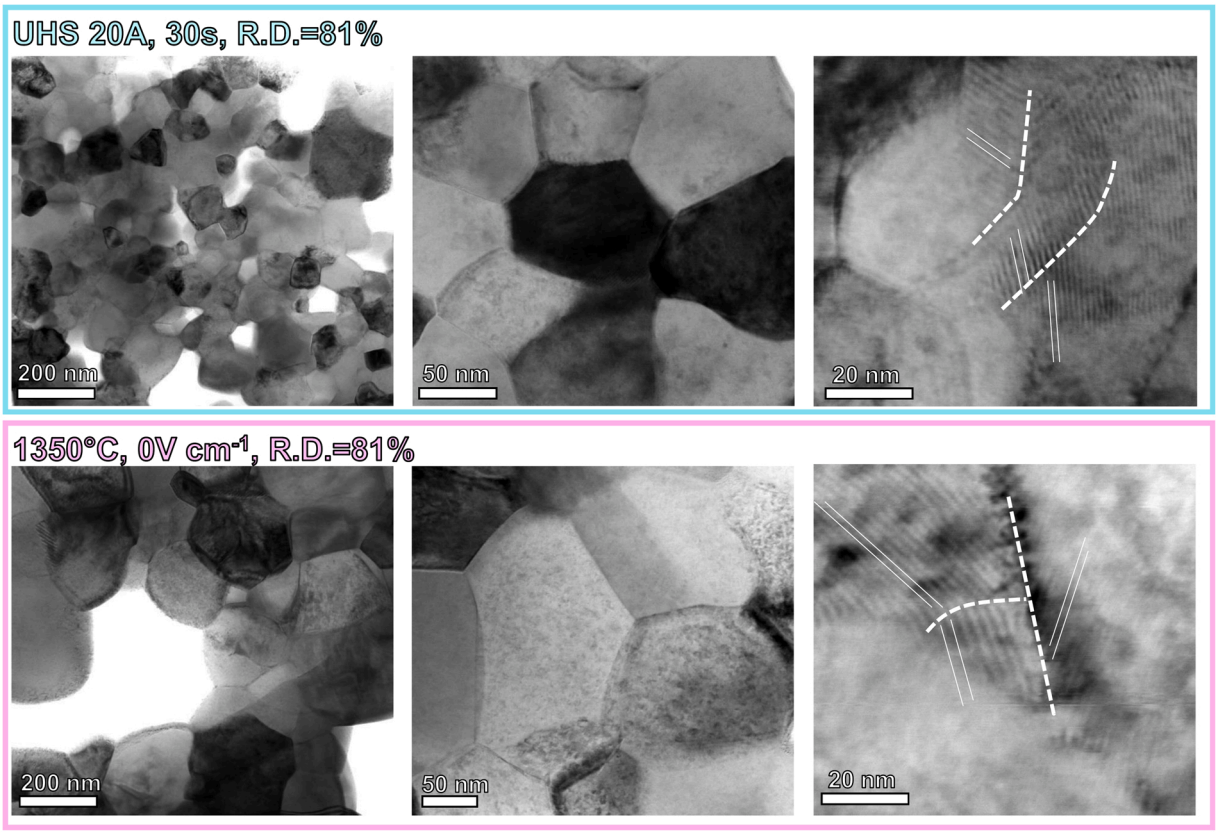

Fig. 9. (a) Bright field S-TEM micrographs of UHS (20 A, 30 s) and conventionally sintered (1350 °C) samples, both samples exhibiting similar relative density.

by observing its microstructure on different regions of the sample. Despite some limited differences can be pointed out, the sample is fairly homogenous with grain size fluctuations below 10 % (Fig. 8).

Fig. 9 reports the S-TEM micrographs of the UHS (20 A) and conventionally sintered (1350 °C) samples both exhibiting a relative density of about 81 %. The micrographs confirm the substantial difference in the microstructure of the two materials, UHS leading to a huge grain refinement compared with conventional firing. Magnification of the grain boundary regions does not reveal obvious differences between the materials, in both cases the grain boundary appears quite "clean" without the formation of thick and clearly detectable disordered regions in the grain boundary vicinity.

From a structural point of view, all the samples with a relative density ≈ 80 % are similar and consist of a mixture of tetragonal and monoclinic zirconia as demonstrated by Raman spectroscopy (peak indexed according to [38,39]) and XRD analyses (Fig. 10). Nevertheless, we can notice that the amount of tetragonal phase is slightly larger in UHS samples, probably due to the much faster cooling process which prevents the conversion to the monoclinic phase upon cooling. Note that despite the tetragonal→monoclinic transition being martensitic, it has already been reported that fast cooling could partially prevent it [40]. Moreover, we should point out that the smaller grain size after UHS can contribute to the stabilization of the tetragonal polymorph [41].

The hardness of UHS and conventionally sintered materials is reported as a function of their relative density in Fig. 11. The hardness increases with density similarly for conventionally sintered and UHS samples, it is therefore independent of the heating rate. No substantial difference with literature data for conventionally sintered and SPS 3YSZ ceramics can be observed [42–44]. As such, the hardness measured in this work after UHS and conventional sintering appears rather robust

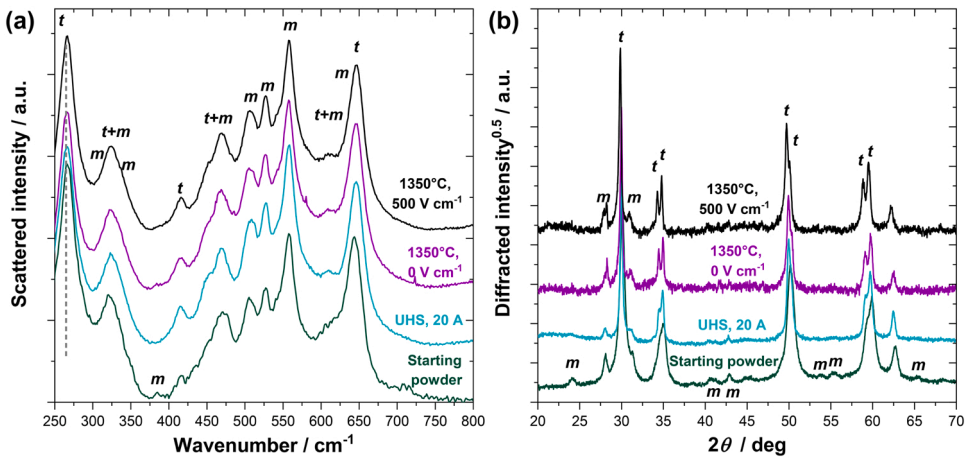

Fig. 10. (a) Raman spectra and (b) XRD patterns of the 81–83 % dense sintered samples. The diagram corresponding to the starting powder are shown for comparison. The dashed line in (a) indicates the cutting edge of the spectrometer.

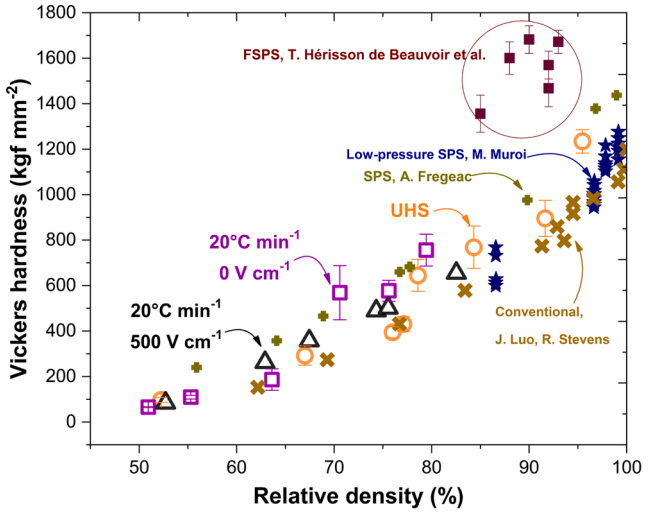

Fig. 11. Vickers hardness of UHS and conventionally sintered 3YSZ (with and without E-field) as a function of the relative density. The average of 10 indentations under 1 kgf in each sample is reported, error bars represent the standard deviations. Literature data taken from [19,42–44] are reported for comparison.

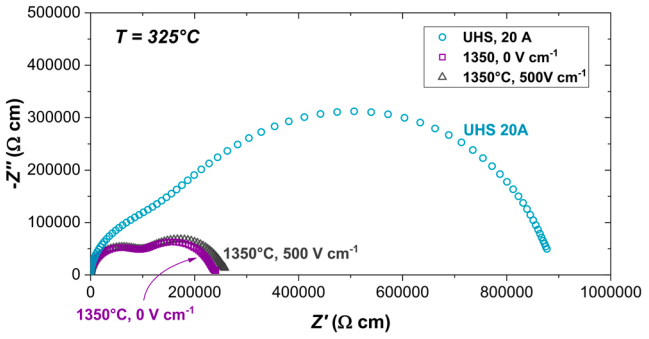

Fig. 12. Nyquist plot of impedance measurements at 325 C from 10^2 to 10^6 Hz for UHS (20 A, 30 s) and conventionally sintered YSZ (with and without E-field). All the samples show similar relative densities (≈ 81–83 %), but different grain size (≈ 90–100 nm for UHS, ≈ 200–250 nm for conventional sintering).

and reliable. It is, however, worth spotting that our results do not match with those obtained on materials produced by flash SPS [19].

The electrochemical impedance of UHS and conventionally sintered samples was measured at various temperatures. Fig. 12 shows the Nyquist plot of a measurement carried out in air at 325 °C. For all samples, two semi-circles can be observed, corresponding to the bulk and grain boundary contributions. For both conventionally heated specimens, no clear difference can be observed, with a total resistivity of 0.24 and 0.25 MΩ cm, thus indicating a similar electrochemical behavior regardless of the application of an electric field during sintering. The behavior of the UHS material is clearly different, with a resistivity of 0.9 MΩ cm and an increase of grain boundary to bulk contribution ratio, in agreement with the finer microstructures observed in Fig. 6.

Data fitting was performed using two R-CPE in series for all samples and at various temperatures from 200 to 400 °C. Fitting results are summarized in Fig. 13. For both conventionally sintered samples, the electrochemical behavior is the same at all temperatures in terms of conductivity, equivalent capacitance, relaxation frequency, and activation energies, both for bulk and grain boundary. Conductivity and grain boundary capacitance are lower in UHS specimens, this being very likely related to the finer microstructure. However, activation energies are similar to those determined for conventionally sintered materials. It is possible to determine grain boundary thickness and specific conductivity as:

$$\delta_{GB} = G \quad \frac{C_{bulk}}{C_{GB}} \tag{1}$$

$$\sigma_{GB}^{sp} = \sigma_{GB} \quad \frac{\delta_{GB}}{G} \tag{2}$$

were δ_{GB} is the grain boundary thickness, G is the mean grain size, C_{bulk} and C_{GB} are the corresponding equivalent capacitances. According to the capacitance data (Fig. 13b), δ_{GB} is found to be 17 and 15 nm for conventionally sintered samples without and with E field, respectively, while it is 18 nm for the UHS sample (data fitted at 300 °C). These data well compare to one previous finding [45], they are slightly higher (13 nm) than that measured on SPS zirconia [19] and very different from data collected on YSZ consolidated by FS [21] and FSPS [19] (about 5 nm). The GB specific conductivity (Fig. 13d) appears invariant with temperature in the considered range and well matches that determined by Bernard-Granger et al. [45].

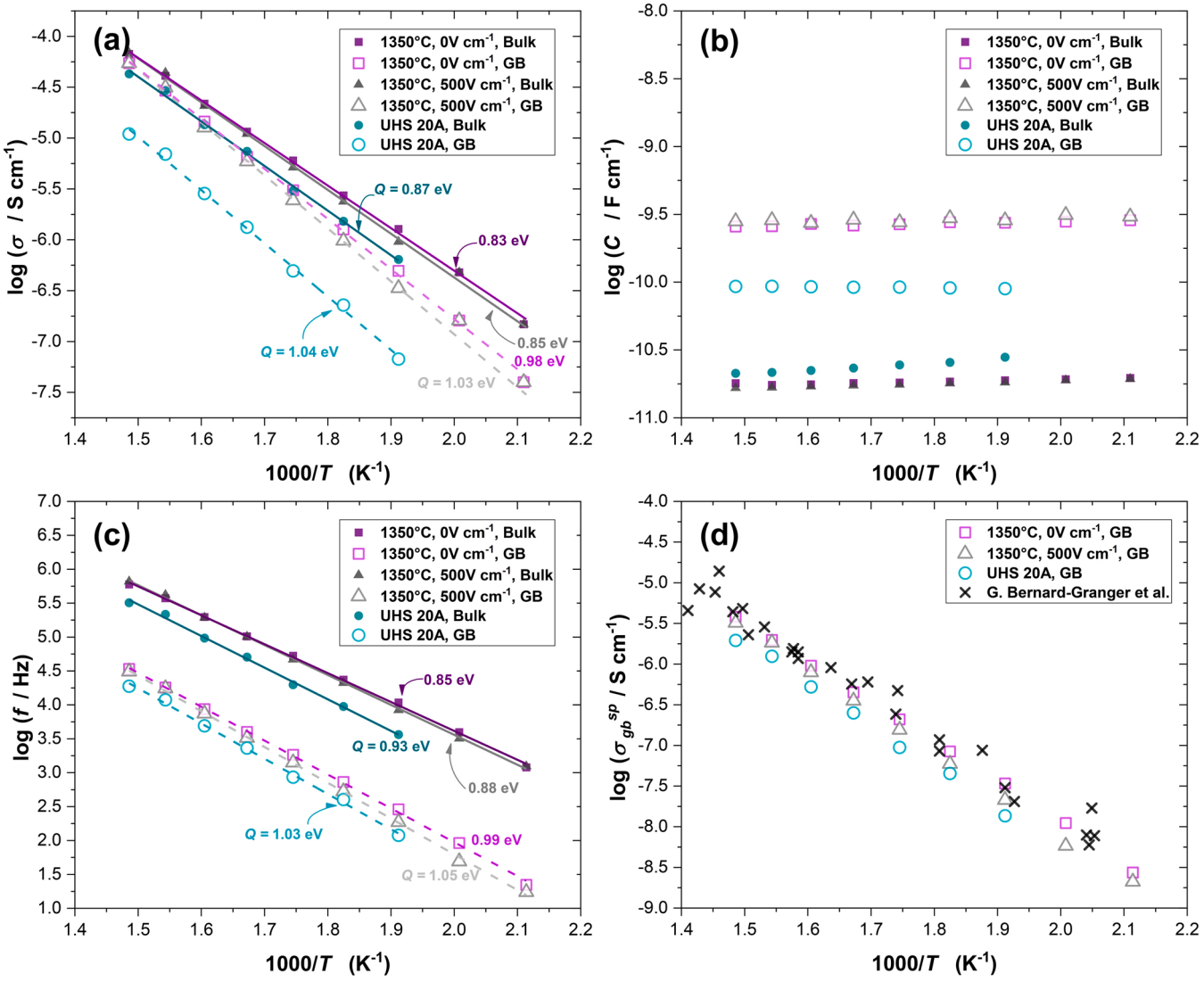

Fig. 13. Data obtained from electrical impedance spectroscopy measurements fits for UHS (20 A, 30 s) and conventionally sintered YSZ (with and without E-field) using two series related R-CPE as equivalent circuits. (a) Conductivity, (b) equivalent capacitance, (c) relaxation frequency, and (d) grain boundary specific conductivity (data from [45] are also shown). *Q* values correspond to the activation energy. All the samples show similar relative densities (≈ 81–83 %), but different grain size (≈ 90–100 nm for UHS, ≈ 200–250 nm for conventional sintering).

4. Discussion

UHS allows an efficient and quite homogeneous (Fig. 8) consolidation of YSZ in a time scale of a few tens of seconds, similar to other rapid sintering technologies, like fast firing [46–50], flash sintering [13,14, 51] and pressure-less SPS [20], thus allowing a remarkable acceleration of the sintering kinetics. The reduction of the sintering temperature in the present work is in the order of 200 °C or more in comparison with conventional heating.

If one considers the microstructure (Figs. 5, 6 and 9) for samples with ≈ 80 % relative density (i.e., the denser sample without any noticeable reduction and or contamination), it is possible to infer that: (i) if compared to conventional heating, UHS allows a remarkable reduction of the grain size (reduction >60% at a density level of 81-83%); (ii) the pore size is definitively smaller and coordinated by more limited number of grains in UHS; (iii) the application of a static electric field of 500 V cm^{-1} does not play a substantial role on sintering. What is observed at points (i) and (ii) is expected to increase the sintering kinetics in UHS and it is therefore at the origin of rapid densification (the sintering rates being proportional to $1/G^n$ with $n = 3$ - 4 depending on the sintering mechanism).

In particular, the smaller and less coordinated pore structure (Figs. 6, 7) is in excellent agreement with previous findings by Ji et al. [16] on flash-sintered YSZ. In fact, they showed that the materials processed by SHS or FS, both characterized by rapid sintering, possess pores with smaller coordination, which are therefore less stable and can be more easily closed. Our results on UHS corroborate their findings and provide additional evidence that the origin of rapid sintering induced by high heating rates is not merely related to differences in the grain size but also in the pore architecture. These microstructural features seem, therefore, general when considering the rapid sintering of YSZ.

Such a result is partially different from what was found in previous UHS experiments on 3YSZ (TZ-3YSB-E, Tosoh, 90 nm), where the master sintering curves (MSC) extrapolated from dilatometry provided a reasonable estimation of the sample density evolution upon UHS [52]. Herein, we observed a substantially enhanced densification in UHS coupled with a very clear difference in the microstructural evolution (Figs. 5, 6, 7 and 9) compared with conventional heating. Note that the assumption that the microstructure is a function of the density, only, is the underlying hypothesis behind the MSC approach which cannot be,

therefore, applied to this specific case. Such different behavior might be triggered by the presence of different impurities elements in the powder composition or, more likely, by the extremely small particle size (≈ 20 nm) of the powders used in this work.

Moreover, we can state that a static electric field of 500 V cm^{-1} plays a minor role on the grain size and densification behavior of 3YSZ nanopowders; hence, the heating rate is the key parameter impacting the material microstructure (Figs. 4–7**)**. No effect of the static field was detected on the electrochemical behavior both in the grain interiors and at the grain boundaries (Fig. 13) nor on the sample hardness (Fig. 11). On these bases, we can exclude that any microstructural features discussed in the previous paragraphs are due to the presence of small E-fields during UHS: the difference in the microstructural evolution and sintering kinetics originates mainly from rapid heating.

Although the effect of UHS on the microstructure is extremely relevant, there are no substantial effects on macroscopic properties like hardness (Fig. 11). These results are substantially different from those previously obtained on zirconia obtained by FSPS [19], where a remarkably higher hardness was measured. The enhanced hardness was attributed to thinner, low-angle, and ordered grain boundaries after FSPS as observed by TEM and EIS. In the present work, the grain boundary properties measured by EIS are similar for both UHS and conventional sintering with an electrochemical grain boundary thickness of ≈ 18 nm. We trust that our EIS results are reliable as the specific grain boundary conductivity (Fig. 13d) is substantially the same for both UHS and conventionally sintered samples, and matches the literature values for materials processed by FSPS and SPS [19,45]. Moreover, no substantial difference in the grain boundary vicinity can be detected by S-TEM when comparing UHS and conventional firing (Fig. 9). In both cases, the grain boundaries appear clean without obvious thick disordered regions. It is worth stressing that EIS and S-TEM observe different features as S-TEM provides an insight into the local conductivity which depends on the oxygen vacancy concentration, whereas S-TEM offers more topological information on the structure related to the degree of order of the material.

On these bases, we can conclude that.

(i) Thinner electrochemical grain boundaries in YSZ obtained by FSPS [19] and FS [21] are *not a universal feature* of rapid sintering as they are not observed in UHS;
(ii) They are not also a field-related effect (as the application of static electric field does not have any effect on EIS results);
(iii) Higher hardness after rapid sintering of YSZ is again *not a universal feature* of rapid sintering as it was observed after FSPS [19] but not here on UHS.

These results corroborate the idea that the thin grain boundary structures originated in FSPS are really the origin of the enhanced hardness, and rapid sintering by UHS causing the simultaneous "disappearance" of thin boundaries and improved hardness.

The origin of the said thin grain boundaries by FSPS and FS is still not clear and a detailed dissertation about this point is outside the scope of the work. However, our results bake the possibility that they are induced by the current flow and electric power dissipation occurring within the sample in the flash state as they do not simply originate from the rapid sintering or the static field.

5. Conclusions

UHS allows rapid densification of 3YSZ nanopowders within 30 s with a relatively homogeneous microstructure. The UHS conditions allow an extraordinary acceleration of the densification kinetics with a substantial decrease of the processing temperature by more than 200 °C compared with conventional heating (regardless of the presence of an electrical field).

3YSZ obtained by UHS shows a finer microstructure (grain size reduced by more than 60% at a density level of 81-83%), and smaller and lower coordination porosity if compared with its conventionally heated counterparts. These phenomena contribute to the accelerated consolidation in UHS and seem to be universally shared by different rapid sintering techniques in YSZ.

On the other hand, the properties of UHS and conventionally sintered materials are rather similar in terms of the electrochemical response of the grain boundaries and Vickers hardness. Such results suggest that the observed modified electrochemical and mechanical properties as well as modified grain boundary structures in the flash process do not simply originate from ultra-rapid heating.

CRediT authorship contribution statement

Mattia Biesuz: Conceptualization, Writing – original draft, Methodology, Visualization, Data curation. **Thomas Hérisson de Beauvoir:** Investigation, Writing – original draft, Formal analysis, Data curation. **Emanuele De Bona:** Investigation, Data curation. **Michele Cassetta:** Investigation, Data curation. **Charles Manière:** Software, Data curation, Visualization. **Vincenzo M. Sglavo:** Supervision, Resources, Writing – review & editing. **Claude Estournès:** Supervision, Resources, Writing – review & editing, Conceptualization.

Declaration of Competing Interest

The authors declare that they have no known competing financial interests or personal relationships that could have appeared to influence the work reported in this paper.

Acknowledgments

This work is supported by the Italian Ministry of Economic Development (Ministero dello Sviluppo Economico, MISE, Italy) within the project "Processo Innovativo per la Ceramica Tecnica - PRINCE", F/310085/01/X56. This research has been funded by the Italian Ministry for University and Research (MUR) through the "Departments of Excellence 2023-27" program (L.232/2016) - awarded to the Department of Industrial Engineering of the University of Trento.

References

[1] M. Biesuz, S. Grasso, V.M. Sglavo, What's new in ceramics sintering? A short report on the latest trends and future prospects, Curr. Opin. Solid State Mater. Sci. 24 (2020) 100868, https://doi.org/10.1016/j.cossms.2020.100868.
[2] E.A. Olevsky, D.V. Dudina, Field-Assisted Sintering, Springer, 2018.
[3] R. Chaim, G. Chevallier, A. Weibel, C. Estournès, Grain growth during spark plasma and flash sintering of ceramic nanoparticles: a review, J. Mater. Sci. 53 (2018) 3087–3105, https://doi.org/10.1007/s10853-017-1761-7.
[4] M. Bram, A. Laptev, T.Prasad Mishra, K. Nur, M. Kindelmann, M. Ihrig, J. Pereira da Silva, R. Steinert, H.Peter Buchkremer, A. Litnovsky, F. Klein, J. Gonzalez-Julian, O. Guillon, Application of electric current assisted sintering techniques for the processing of advanced materials, Adv. Eng. Mater. (2020), https://doi.org/10.1002/adem.202000051.
[5] S. Grasso, Y. Sakka, G. Maizza, Electric current activated/assisted sintering (ECAS): a review of patents 1906–2008, Sci. Technol. Adv. Mater. 10 (2009) 053001.
[6] K.I. Rybakov, E.A. Olevsky, E.V. Krikun, Microwave sintering: Fundamentals and modeling, J. Am. Ceram. Soc. 96 (2013) 1003–1020, https://doi.org/10.1111/jace.12278.
[7] M. Cologna, B. Rashkova, R. Raj, Flash sintering of nanograin zirconia in <5 s at 850°C, J. Am. Ceram. Soc. 93 (2010) 3556–3559.
[8] R.I. Todd, Flash sintering of ceramics: a short review, Proc. IV Adv. Ceram. Appl. Conf. (2017) 1–12.
[9] M. Biesuz, V.M. Sglavo, Flash sintering of ceramics, J. Eur. Ceram. Soc. 39 (2019) 115–143, https://doi.org/10.1016/j.jeurceramsoc.2018.08.048.
[10] G.M. Jones, M. Biesuz, W. Ji, S.F. John, C. Grimley, C. Manière, C.E.J. Dancer, Promoting microstructural homogeneity during flash sintering of ceramics through thermal management, MRS Bull. 46 (2021) 59–66, https://doi.org/10.1557/s43577-020-00010-2.
[11] S. Grasso, T.G. Saunders, Spark plasma sintering in a flash, Am. Ceram. Soc. Bull. 95 (2016) 32–34.

[12] S. Grasso, T. Saunders, H. Porwal, B. Milsom, A. Tudball, M. Reece, Flash Spark Plasma Sintering (FSPS) of alpha and beta SiC, J. Am. Ceram. Soc. 99 (2016) 1534–1543, https://doi.org/10.1111/jace.14158.
[13] Y. Zhang, J. Nie, J.M. Chan, J. Luo, Probing the densification mechanisms during flash sintering of ZnO, Acta Mater. 125 (2017) 465–475.
[14] W. Ji, B. Parker, S. Falco, J.Y. Zhang, Z.Y. Fu, R.I. Todd, Ultra-fast firing: Effect of heating rate on sintering of 3YSZ, with and without an electric field, J. Eur. Ceram. Soc. 37 (2017) 2547–2551.
[15] M.N. Rahaman, Ceramics Processing and Sintering, 2nd ed., 2003, pp. 514–536, https://doi.org/10.1201/9781315274126.
[16] W. Ji, J. Zhang, W. Wang, Z. Fu, R.I. Todd, The microstructural origin of rapid densification in 3YSZ during ultra-fast firing with or without an electric field, J. Eur. Ceram. Soc. 40 (2020) 5829–5836, https://doi.org/10.1016/j.jeurceramsoc.2020.07.027.
[17] Y.-M. Chiang, D. Birnie, P.W.D. Kingery, Physical Ceramics: Principles for Ceramic Science and Engineering, Wiley, 1997.
[18] J. Zhang, F. Meng, R.I. Todd, Z. Fu, The nature of grain boundaries in alumina fabricated by fast sintering, Scr. Mater. 62 (2010) 658–661.
[19] T. Hérisson de Beauvoir, Z. Ghomari, G. Chevallier, A. Flaureau, A. Weibel, C. Elissalde, F. Mauvy, R. Chaim, C. Estournès, Flash spark plasma sintering of 3YSZ: modified sintering pathway and impact on grain boundary formation, J. Eur. Ceram. Soc. 41 (2021) 7762–7770, https://doi.org/10.1016/j.jeurceramsoc.2021.08.013.
[20] A. Kocjan, M. Logar, Z. Shen, The agglomeration, coalescence and sliding of nanoparticles, leading to the rapid sintering of zirconia nanoceramics, Sci. Rep. 7 (2017) 2541, https://doi.org/10.1038/s41598-017-02760-7.
[21] J.C. M'Peko, J.S.C. Francis, R. Raj, Impedance spectroscopy and dielectric properties of flash versus conventionally sintered yttria-doped zirconia electroceramics viewed at the microstructural level, J. Am. Ceram. Soc. 96 (2013) 3760–3767, https://doi.org/10.1111/jace.12567.
[22] C. Wang, W. Ping, Q. Bai, H. Cui, R. Hensleigh, R. Wang, A.H. Brozena, Z. Xu, J. Dai, Y. Pei, C. Zheng, G. Pastel, J. Gao, X. Wang, H. Wang, J.-C. Zhao, B. Yang, X. (Rayne Zheng, J. Luo, Y. Mo, B. Dunn, L. Hu, A general method to synthesize and sinter bulk ceramics in seconds, Science 368 (1979) (2020) 521–526, https://doi.org/10.1126/science.aaz7681.
[23] T.P. Mishra, S. Wang, C. Lenser, D. Jennings, M. Kindelmann, W. Rheinheimer, C. Broeckmann, M. Bram, O. Guillon, Ultra-fast high-temperature sintering of strontium titanate, Acta Mater. 231 (2022) 117918, https://doi.org/10.1016/j.actamat.2022.117918.
[24] L. Spiridigliozzi, G. Dell'Agli, S. Esposito, P. Rivolo, S. Grasso, V.M. Sglavo, M. Biesuz, Ultra-fast high-temperature sintering (UHS) of Ce0.2Zr0.2Y0.2Gd0.2La0.2O2−δ fluorite-structured entropy-stabilized oxide (F-ESO), Scr. Mater. 214 (2022) 114655, https://doi.org/10.1016/j.scriptamat.2022.114655.
[25] F. Zuo, Q. Wang, Z.Q. Yan, M. Kermani, S. Grasso, G.L. Nie, B.B. Jiang, F.P. He, H. T. Lin, L.G. Wang, Upscaling ultrafast high-temperature sintering (UHS) to consolidate large-sized and complex-shaped ceramics, Scr. Mater. 221 (2022) 114973, https://doi.org/10.1016/j.scriptamat.2022.114973.
[26] M. Biesuz, A. Galotta, A. Motta, M. Kermani, S. Grasso, J. Vontorová, V. Tyrpekl, M. Vilémová, V.M. Sglavo, Speedy bioceramics: rapid densification of tricalcium phosphate by ultrafast high-temperature sintering, Mater. Sci. Eng.: C 127 (2021) 112246, https://doi.org/10.1016/j.msec.2021.112246.
[27] R.-X. Luo, M. Kermani, Z.-L. Guo, J. Dong, C.-F. Hu, F. Zuo, S. Grasso, B.-B. Jiang, G.-L. Nie, Z.-Q. Yan, Q. Wang, Y.-L. Gan, F.-P. He, H.-T. Lin, Ultrafast high-temperature sintering of silicon nitride: A comparison with the state-of-the-art techniques, J. Eur. Ceram. Soc. 41 (2021) 6338–6345, https://doi.org/10.1016/j.jeurceramsoc.2021.06.021.
[28] H.W. Li, Y.P. Zhao, G.Q. Chen, M.H. Li, Z.F. Wei, X.S. Fu, W.L. Zhou, SiC-based ceramics with remarkable electrical conductivity prepared by ultrafast high-temperature sintering, J. Eur. Ceram. Soc. (2022), https://doi.org/10.1016/j.jeurceramsoc.2022.12.025.
[29] Y. Sun, L. Zhao, R.-F. Guo, P. Shen, Cr3C2 assisted ultrafast high-temperature sintering of TiC, J. Eur. Ceram. Soc. 43 (2023) 5458–5465, https://doi.org/10.1016/j.jeurceramsoc.2023.05.031.
[30] A. Alemayehu, M. Biesuz, K.Y. Javan, A. Tkach, P.M. Vilarinho, V.M. Sglavo, V. Tyrpekl, Ultrafast high-temperature sintering of gadolinia-doped ceria, J. Eur. Ceram. Soc. 43 (2023) 4837–4843, https://doi.org/10.1016/j.jeurceramsoc.2023.04.025.
[31] L. Fu, J. Wu, S.K.M. Sathyanath, B. Wang, K. Leifer, H. Engqvist, S. Grasso, W. Xia, Far from equilibrium ultrafast high-temperature sintering of ZrO 2 –SiO 2 nanocrystalline glass–ceramics, J. Am. Ceram. Soc. 106 (2023) 4005–4012, https://doi.org/10.1111/jace.19055.
[32] F. Ye, F. Meng, T. Luo, H. Qi, The CMAS corrosion behavior of high-entropy (Y0.2Dy0.2Er0.2Tm0.2Yb0.2)4Hf3O12 hafnate material prepared by ultrafast high-temperature sintering (UHS), J. Eur. Ceram. Soc. 43 (2023) 2185–2195, https://doi.org/10.1016/j.jeurceramsoc.2022.12.011.
[33] Z. Lin, X. Zhao, C. Wang, Q. Dong, J. Qian, G. Zhang, A.H. Brozena, X. Wang, S. He, W. Lin, G. Chen, Y. Pei, C. Zheng, B.C. Clifford, M. Hong, Y. Wu, B. Yang, J. Luo, P. Albertus, L. Hu, Rapid pressureless sintering of glasses, Small 18 (2022) 2107951, https://doi.org/10.1002/smll.202107951.
[34] S. Mondal, J.D.S. Lombard, S. Gollapudi, C. Tallon, J. Li, D. Viehland, Ultrafast high-temperature sintering of ZrB 2, J. Am. Ceram. Soc. (2023), https://doi.org/10.1111/jace.19445.
[35] J. Wu, M. Kermani, D. Zhu, J. Li, Y. Lin, C. Hu, S. Grasso, Carbon free ultra-fast high temperature sintering of translucent zirconia, Scr. Mater. 210 (2022) 114476, https://doi.org/10.1016/j.scriptamat.2021.114476.
[36] S. Bhandari, C. Manière, F. Sedona, E. De Bona, V.M. Sglavo, P. Colombo, L. Fambri, M. Biesuz, G. Franchin, Ultra-rapid debinding and sintering of additively manufactured ceramics by ultrafast high-temperature sintering, J. Eur. Ceram. Soc. 44 (2024) 328–340, https://doi.org/10.1016/j.jeurceramsoc.2023.08.040.
[37] E. De Bona, C. Manière, V.M. Sglavo, M. Biesuz, Ultrafast high-temperature sintering (UHS) of ZrB2-based materials, J. Eur. Ceram. Soc. 44 (2024) 567–573, https://doi.org/10.1016/j.jeurceramsoc.2023.09.007.
[38] D.A. Daramola, M. Muthuvel, G.G. Botte, Density functional theory analysis of Raman frequency modes of monoclinic zirconium oxide using gaussian basis sets and isotopic substitution, J. Phys. Chem. B 114 (2010) 9323–9329, https://doi.org/10.1021/jp9077135.
[39] T. Merle, R. Guinebretiere, A. Mirgorodsky, P. Quintard, Polarized Raman spectra of tetragonal pure ZrO2 measured on epitaxial films, Phys. Rev. B 65 (2002) 144302, https://doi.org/10.1103/PhysRevB.65.144302.
[40] G. Roncallo, E. Barbareschi, G. Cacciamani, E. Vacchieri, Effect of cooling rate on phase transformation in 6–8 wt % YSZ APS TBCs, Surf. Coat. Technol. 412 (2021) 127071, https://doi.org/10.1016/j.surfcoat.2021.127071.
[41] A. Suresh, M.J. Mayo, W.D. Porter, C.J. Rawn, Crystallite and grain-size-dependent phase transformations in yttria-doped zirconia, J. Am. Ceram. Soc. 86 (2003) 360–362, https://doi.org/10.1111/j.1151-2916.2003.tb00025.x.
[42] A. Fregeac, F. Ansart, S. Selezneff, C. Estournès, Relationship between mechanical properties and microstructure of yttria stabilized zirconia ceramics densified by spark plasma sintering, Ceram. Int 45 (2019) 23740–23749, https://doi.org/10.1016/j.ceramint.2019.08.090.
[43] J. Luo, R. Stevens, Porosity-dependence of elastic moduli and hardness of 3Y-TZP ceramics, Ceram. Int 25 (1999) 281–286, https://doi.org/10.1016/S0272-8842(98)00037-6.
[44] M. Muroi, G. Trotter, P.G. McCormick, M. Kawahara, M. Tokita, Preparation of nano-grained zirconia ceramics by low-temperature, low-pressure spark plasma sintering, J. Mater. Sci. 43 (2008) 6376–6384, https://doi.org/10.1007/s10853-008-2559-4.
[45] G. Bernard-Granger, C. Guizard, S. Surblé, G. Baldinozzi, A. Addad, Spark plasma sintering of a commercially available granulated zirconia powder—II. Microstructure after sintering and ionic conductivity, Acta Mater. 56 (2008) 4658–4672, https://doi.org/10.1016/j.actamat.2008.05.031.
[46] M.N. Rahaman, Ceramic Processing and Sintering, Marcel Dekker, New York, USA, 1996.
[47] M. Biesuz, L. Spiridigliozzi, M. Frasnelli, G. Dell'Agli, V.M.V.M. Sglavo, Rapid densification of Samarium-doped Ceria ceramic with nanometric grain size at 900–1100°C, Mater. Lett. 190 (2017) 17–19, https://doi.org/10.1016/j.matlet.2016.12.132.
[48] M.S. Sectol, I. Road, G.U. Olx, Fast Firing of Electroceramics, 1999, pp. 159–166.
[49] V. Esposito, E. Traversa, Design of electroceramics for solid oxides fuel cell applications: Playing with ceria, J. Am. Ceram. Soc. 91 (2008) 1037–1051, https://doi.org/10.1111/j.1551-2916.2008.02347.x.
[50] W. Lerdprom, R.K. Chinnam, D.D. Jayaseelan, W.E. Lee, Porcelain production by direct sintering, J. Eur. Ceram. Soc. 36 (2016) 4319–4325.
[51] S. Grasso, T. Saunders, H. Porwal, B. Milsom, A. Tudball, M. Reece, I.W. Chen, Flash Spark Plasma Sintering (FSPS) of α and β SiC, J. Am. Ceram. Soc. 99 (2016) 1534–1543, https://doi.org/10.1111/jace.14158.
[52] J. Dong, V. Pouchly, M. Biesuz, V. Tyrpekl, M. Vilémová, M. Kermani, M. Reece, C. Hu, S. Grasso, Thermally-insulated ultra-fast high temperature sintering (UHS) of zirconia: A master sintering curve analysis, Scr. Mater. 203 (2021) 114076, https://doi.org/10.1016/j.scriptamat.2021.114076.